

---

# Protecting the Intellectual Property of Diffusion Models by the Watermark Diffusion Process

---

Sen Peng<sup>1</sup> Yufei Chen<sup>1</sup> Cong Wang<sup>1</sup> Xiaohua Jia<sup>1</sup>

## Abstract

Diffusion models have emerged as state-of-the-art deep generative architectures with the increasing demands for generation tasks. Training large diffusion models for good performance requires high resource costs, making them valuable intellectual properties to protect. While most of the existing ownership solutions, including watermarking, mainly focus on discriminative models. This paper proposes **WDM**, a novel watermarking method for diffusion models, including watermark embedding, extraction, and verification. WDM embeds the watermark data through training or fine-tuning the diffusion model to learn a **Watermark Diffusion Process (WDP)**, different from the standard diffusion process for the task data. The embedded watermark can be extracted by sampling using the shared reverse noise from the learned WDP without degrading performance on the original task. We also provide theoretical foundations and analysis of the proposed method by connecting the WDP to the diffusion process with a modified Gaussian kernel. Extensive experiments are conducted to demonstrate its effectiveness and robustness against various attacks.

## 1. Introduction

Deep generative models are drawing significant attention in academia and industry due to the large demand for applications. Among them, diffusion models is a kind of architecture inspired by the diffusion process in non-equilibrium thermodynamics [1]. Recent studies [2; 3; 4] have shown that diffusion models can generate samples with higher quality and diversity compared to classic architectures like Generative Adversarial Network (GAN) [5; 6] and Variational Auto-Encoder (VAE) [7; 8]. Large well-trained diffusion models, such as Stable Diffusion [9], are becoming foun-

dations of various downstream services. The widespread use of diffusion models has intensified the imperative to protect their Intellectual Property (IP). Firstly, these models represent valuable digital assets for developers who invest significant time and financial resources in obtaining high-performance models [10]. Secondly, the unauthorized dissemination of well-trained diffusion models can give rise to ethical concerns, such as the potential model misuse for generating disinformation.

Deep Neural Network (DNN) watermarking is a common solution for model IP protection [11; 12]. It embeds specific information as the watermark into models before their deployment. The embedded watermark can be extracted from the suspected model to verify the existence of IP violations. DNN watermarking can be classified into static and dynamic approaches based on where the watermark is embedded. Static watermarking [13; 14; 15; 16] typically embeds a specific pattern into the model's static content as the watermark, like regularising the model's parameters to follow a certain distribution. In static methods, watermark extraction needs complete access to the suspected model, which requires the white-box setting. In contrast, dynamic watermarking [17; 18; 19; 20; 21; 22; 23; 24; 25; 26] embeds a specific pattern into the model's dynamic content, like its behavior (or functionality) as the watermark, typically exploiting the adversarial example and backdoor attack of DNN models. Watermark extraction of dynamic methods usually needs inference results instead of access to the suspected model, which can be processed under the black-box setting. However, most of the current research on DNN watermarking focuses only on discriminative models. The research on watermarking generative models, especially recently emerged diffusion models, is still limited. The challenges mainly involve 1) the difficulty of controlling the generation process while not affecting performance on the original task [27; 28] and 2) limited input to generative models (no input is needed for unconditional generative models). Some recent studies have explored watermarking techniques for generative models [29; 27; 30; 28]. However, these studies primarily either cannot be applied to diffusion models or focus on embedding the watermark to the task generation results.

---

<sup>1</sup>Department of Computer Science, City University of Hong Kong, Kowloon, Hong Kong SAR.

In this paper, we propose the WDM, a novel watermarking scheme for diffusion models by learning the watermark diffusion process without leaking the watermark during task generation. The key of WDM is to let the protected model obtains the ability to generate samples following a different data distribution as the watermark, which mainly consists of three stages (as shown Figure. 1). In the *watermark embedding stage*, we firstly sample a watermark dataset from that target distribution as the watermark carrier. We then construct the **Watermark Diffusion Process (WDP)** based on the standard diffusion process for samples in the watermark data distribution. We embed the watermark into the host model by training or fine-tuning it to learn two diffusion processes together: a standard diffusion process for the task data and a WDP for the watermark data. The optimization objective for the WDP can be simplified by proving the equivalence between a WDP with specific configurations satisfied and a **Diffusion Process with the Modified Gaussian kernel (MDP)**. In the *watermark extraction stage*, we extract the watermark through a standard reverse diffusion process for the watermark data, using the shared reverse noise learned by the WDP. Finally, in the *watermark verification stage*, we present the conclusion about IP violation based on the confidence score given by watermark similarity comparison and hypothesis testing.

To summarize, the primary contributions of this work are 1) We propose a novel scheme to protect the IP for diffusion models through the WDP including the watermark embedding, extraction and verification. 2) We give the theoretical foundations and analysis for the optimization objective during training the model to learn the WDP by connecting the WDP with an MDP. 3) We conduct extensive experiments to demonstrate the effectiveness and robustness of WDM against various attacks.

## 2. Related Work

### 2.1. Diffusion Probabilistic Models

Diffusion probabilistic models (DMs for short) are latent variable generative models inspired by the diffusion process in non-equilibrium thermodynamics [1]. The diffusion process describes data transition from one distribution to another through a finite Markov chain. The forward process diffuses its original distribution to a noisy distribution by gradually adding noises to data samples. Conversely, the reverse process gradually removes noises from the noisy distribution to recover the data following the task distribution. As long as each state transition in the forward diffusion process is sufficiently small with specific transition kernels such as the Gaussian kernel, it can be proved that the transition kernels in the reverse process share the same form [1; 31]. Later, Ho et al. proposed Denoising Diffusion Probabilistic Models (DDPMs) to simplify the optimization objective

in training diffusion models [2], and Song et al. linked the diffusion models with score-based models inspired by Langevin dynamics [32; 31]. Further studies are conducted to speed up the sampling process [33] and improve the data generalization [34].

### 2.2. DNN Watermarking

DNN watermarking has been developed for years to protect the copyright of DNN models. It exploits the redundancy of the model's parameter space which has multiple local optimal. Parameters of the model are altered from one local optimal to another during watermark embedding, making it feasible to achieve without significantly affecting its original functionality.

**Watermarking Discriminative Models** Watermarking can be categorized into static and dynamic approaches for discriminative models depending on where the watermark is embedded [12]. Static watermarking [13; 14; 15; 16] defines the watermark as a specific pattern in its static content, such as a particular distribution that the model's parameters follow. In contrast, dynamic watermarking [17; 18; 19; 20; 21; 22; 23; 24; 25; 26] designs the watermark as a specific pattern in model's dynamic contents, like its behavior. It typically exploits the adversarial example [17] and backdoor attack [19; 20; 23; 26; 25] of DNN models to construct the specific behavior as the watermark, where the watermark dataset contains trigger samples and pre-defined labels.

**Watermarking Generative Models** Watermarking generative models is more challenging due to the difficulty of controlling the generative process while not affecting the original task. Previous studies [29; 30; 27] propose methods to watermark GANs by constructing mappings between trigger inputs and outputs given by the generator through regularization constraints in the training objective. However, these methods cannot be applied to DMs since regularization cannot directly control the diffusion process's inherent randomness. Previous research [35] has explored the backdoor attacks of DMs by modifying the training optimization objective and triggering it through sampling from the noise with a specific distribution. However, watermarking methods for DMs based on this backdoor attack have not been developed. A recent study [28] presents a watermarking scheme for DMs, where an encoder is trained to implant the watermark into task data embedding and a decoder to extract the watermark from the task generation results. In comparison, our proposed method learns to generate the watermark data through a WDP which does not affect the standard diffusion process for task data. To our best knowledge, this is the first work that provides an ownership resolution of DMs by implanting a different diffusion process for the watermark data.

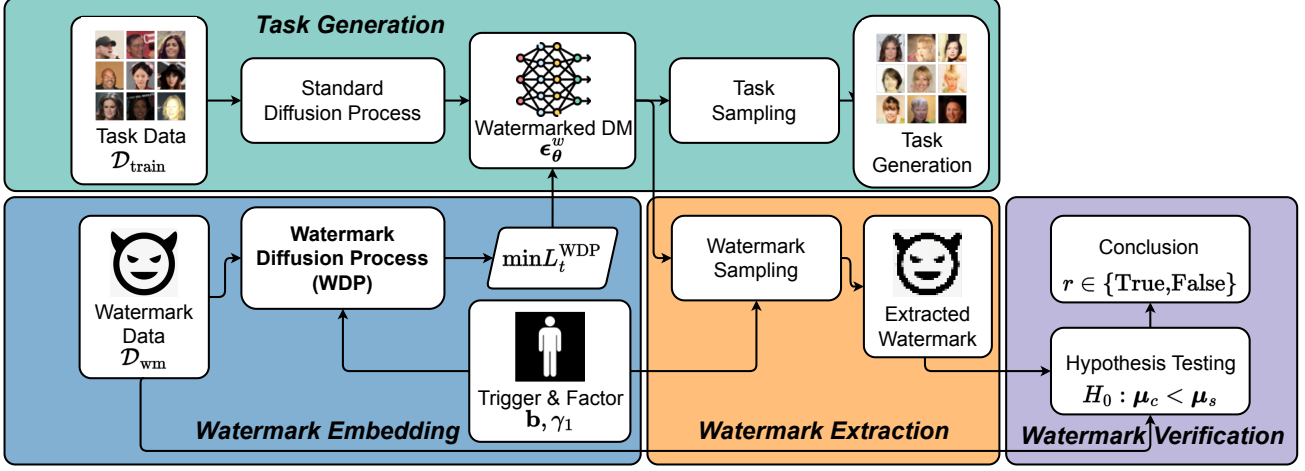


Figure 1: Framework of the proposed watermarking method WDM. **Top:** The task data  $\mathcal{D}_{\text{train}}$  is learned by the standard diffusion process in the watermarked DM, which is the same as the training and sampling of a standard DM. **Bottom:** The watermark data  $\mathcal{D}_{\text{wm}}$  is embedded by the WDP into the watermarked DM with the trigger  $\mathbf{b}$  and trigger factor  $\gamma_1$ . It can be extracted through watermark sampling, and verified through similarity comparison and hypothesis testing.

### 3. Preliminary and Problem Definition

#### 3.1. Denoising Diffusion Probabilistic Models

In this paper, we choose the unconditional DDPM [2] as our target diffusion model since it simplifies the training objective in [1] and becomes a fundamental work for many follow-up researches. In DDPM, the forward diffusion process describes how to gradually transition a data sample  $\mathbf{x}_0 \sim q(\mathbf{x})$  from a given distribution to approximate the isotropic Gaussian distribution  $\mathcal{N}(0, 1)$ . This is achieved through a Gaussian transition kernel as

$$q(\mathbf{x}_t | \mathbf{x}_{t-1}) = \mathcal{N}(\mathbf{x}_t; \sqrt{\alpha_t} \mathbf{x}_{t-1}, (1 - \alpha_t) \mathbf{I}), \quad (1)$$

where  $\alpha_t = 1 - \beta_t$  and  $\{\beta_t \in (0, 1)\}_{t=1}^T$  is the variance schedule that controls the diffusion step size. By denoting  $\prod_{i=1}^t \alpha_i$  as  $\bar{\alpha}_t$ , we can represent  $\mathbf{x}_t$  using the reparameterization trick as

$$\mathbf{x}_t = \sqrt{\bar{\alpha}_t} \mathbf{x}_0 + \sqrt{1 - \bar{\alpha}_t} \boldsymbol{\epsilon}, \quad (2)$$

where  $\boldsymbol{\epsilon} \sim \mathcal{N}(0, 1)$ . The reverse diffusion process also has a transition kernel with Gaussian form as  $q(\mathbf{x}_{t-1} | \mathbf{x}_t, \mathbf{x}_0) = \mathcal{N}(\mathbf{x}_{t-1}; \tilde{\boldsymbol{\mu}}_t(\mathbf{x}_t, \mathbf{x}_0), \tilde{\sigma}_t \mathbf{I})$ . For the reverse diffusion process,  $p_{\theta}(\mathbf{x}_{t-1} | \mathbf{x}_t) = \mathcal{N}(\mathbf{x}_{t-1}; \boldsymbol{\mu}_{\theta}(\mathbf{x}_t, t), \boldsymbol{\Sigma}_{\theta}(\mathbf{x}_t, t))$  is used to approximate this posterior probability. In DDPM, the variance of the approximated probability is fixed the same as  $\boldsymbol{\Sigma}_{\theta} = \sigma_t = \beta_t \mathbf{I}$  for simplification. Its mean can be predicted using a machine learning model  $\boldsymbol{\epsilon}_{\theta}$  as

$$\boldsymbol{\mu}_{\theta}(\mathbf{x}_t, t) = \frac{1}{\sqrt{\alpha_t}} (\mathbf{x}_t - \frac{1 - \alpha_t}{\sqrt{1 - \bar{\alpha}_t}} \boldsymbol{\epsilon}_{\theta}(\mathbf{x}_t, t)), \quad (3)$$

where we can sample from the noisy distribution by

$$\mathbf{x}_{t-1} = \frac{1}{\sqrt{\alpha_t}} (\mathbf{x}_t - \frac{1 - \alpha_t}{\sqrt{1 - \bar{\alpha}_t}} \boldsymbol{\epsilon}_{\theta}(\mathbf{x}_t, t)) + \sigma_t \mathbf{z} \quad (4)$$

with  $\mathbf{z} \sim \mathcal{N}(0, 1)$ . The training objective of  $\boldsymbol{\epsilon}_{\theta}$  is similar to minimizing the negative log-likelihood in VAE [7; 8], which can be optimized using the variational lower bound as

$$L_t^{\text{simple}} = \mathbb{E}_{t \sim [1, T], \mathbf{x}_0, \boldsymbol{\epsilon}_t} \left[ \|\boldsymbol{\epsilon}_t - \boldsymbol{\epsilon}_{\theta}(\sqrt{\bar{\alpha}_t} \mathbf{x}_0 + \sqrt{1 - \bar{\alpha}_t} \boldsymbol{\epsilon}_t, t)\|^2 \right], \quad (5)$$

where  $\boldsymbol{\epsilon}_t$  is the reverse noise at  $t$ .

#### 3.2. Problem Definition

**Threat Model.** This paper explores the threat model of defending stealing towards diffusion models. Specifically, we consider the scenario where an owner trains a diffusion model on a task dataset  $\mathcal{D}_{\text{train}}$  and obtains the host model  $\boldsymbol{\epsilon}_{\theta}^o$  for usage. An attacker successfully steals a copy of the host model as a stolen model, declares the copyright of it without referring to  $\boldsymbol{\epsilon}_{\theta}^o$ , which harms the IP rights of the model owner. The owner instead trains or fine-tunes  $\boldsymbol{\epsilon}_{\theta}^o$  to obtain a watermarked model  $\boldsymbol{\epsilon}_{\theta}^w$  with a watermark dataset  $\mathcal{D}_{\text{wm}}$ . The owner keeps the embedded watermark and the used trigger as secrets. After observing a suspected model  $\boldsymbol{\epsilon}_{\theta}^s$  from the attacker, the owner can extract the watermark and verify whether it is stolen by comparing it with the embedded one. Since unconditional DMs need no input for inference, we assume the owner can obtain full access to  $\boldsymbol{\epsilon}_{\theta}^s$  or entrust the extraction and verification process to a trusted third party.

**Defense Goal.** Given dataset  $\mathcal{D}_{\text{train}}$  and  $\mathcal{D}_{\text{wm}}$ , a complete watermarking scheme contains three sub-algorithms. Specifically:

1. **Watermark Embedding**  $f_{\text{embed}}$ : It embeds the watermark  $\mathbf{a}$  into the host model  $\boldsymbol{\epsilon}_{\theta}^o$  to obtain the watermarked model  $\boldsymbol{\epsilon}_{\theta}^w$  with a trigger  $\mathbf{b}$  as  $f_{\text{embed}}(\boldsymbol{\epsilon}_{\theta}^o, \mathbf{a}, \mathbf{b}) \rightarrow \boldsymbol{\epsilon}_{\theta}^w$ .

2. **Watermark Extraction**  $f_{\text{extract}}$ : It can extract the watermark  $\hat{\mathbf{a}}$  with the trigger  $\mathbf{b}$  from the suspected model as  $f_{\text{extract}}(\epsilon_{\theta}^s, \mathbf{b}) \rightarrow \hat{\mathbf{a}}$  for a suspected model  $\epsilon_{\theta}^s$  from the attacker.
3. **Watermark Verification**  $f_{\text{verify}}$ : It compares the extracted watermark with the embedded one and outputs a verification result  $r$  for as  $f_{\text{verify}}(\mathbf{a}, \hat{\mathbf{a}}) \rightarrow r \in \{\text{True}, \text{False}\}$ .

In this paper, we propose a complete watermarking method  $\mathcal{F}_w = \{f_{\text{embed}}, f_{\text{extract}}, f_{\text{verify}}\}$  that enables the owner to prevent potential IP violations from attackers. The proposed method needs to achieve three goals:

1. **Model Fidelity**: The watermarking method does not significantly degrade the task generation performance of the model.
2. **Watermark Detectability**: The target embedded watermark can be extracted from a watermarked model, and its existence can be verified.
3. **Watermark Robustness**: The embedded watermark should be resistant to removing attacks. The watermark can be extracted from the modified models and its existence can be verified.

The development of such a complete watermarking technique can provide the necessary security for DMs, enabling the safe distribution to third parties without IP violations.

## 4. Proposed Method

In this section, we first define the diffusion process with the modified Gaussian kernel and theoretically demonstrate its simplified optimization objective. We then define the watermark diffusion process and prove that a WDP is an MDP with specific configurations satisfied. We propose the watermark embedding algorithm by training a watermarked diffusion model (or fine-tuning the pre-trained host one) to learn a standard diffusion process for task data distribution and a WDP for watermark data distribution together. The watermark trigger can be selected with prior knowledge or randomly generated through a Pseudo Random Function (PRF) given the secret key. Since the WDP shares the same reverse noise as the standard diffusion process for the watermark data, watermark extraction can be considered as the sampling process using the reverse noise predicted by the learned WDP instead of the standard diffusion process. Finally, we propose the watermark verification algorithm by comparing the similarity and hypothesis testing for both settings, where the watermark dataset contains only one or multiple samples.

### 4.1. Diffusion Process with the Modified Gaussian Kernel

In the proposed method, we utilize the ability to generate watermark distribution  $q(\mathbf{x}^w)$  as the watermark to embed into diffusion models. In practice, we use the watermark dataset  $\mathcal{D}_{\text{wm}}$  consisting samples  $\mathbf{x}_0^w \sim q(\mathbf{x}^w)$  as the watermark carrier. To avoid leaking the watermark during sampling task data, we embed the watermark through a diffusion process different from the standard one. Inspired by the multiplying distributions part in [1], we first define the diffusion process with the modified Gaussian kernel for the data distribution  $q(\mathbf{x})$ .

**Definition 1.** For samples  $\mathbf{x}_0 \sim q(\mathbf{x})$ , we define the diffusion process in finite timesteps  $\{1, \dots, T\}$ , which have the following forward transition kernel

$$q(\mathbf{x}_t | \mathbf{x}_{t-1}) = \mathcal{N}(\mathbf{x}_t; \sqrt{\alpha_t}(\mathbf{x}_{t-1} + \phi_t), \eta^2(1 - \alpha_t)\mathbf{I}), \quad (6)$$

where  $\phi_t$  is the constant schedule and  $\eta \in (0, 1)$ , as a diffusion process with the modified Gaussian kernel (an MDP).

It is necessary to obtain the reverse transition kernel  $q(\mathbf{x}_{t-1} | \mathbf{x}_t)$  of an MDP for generating samples from a noisy distribution using an MDP. We construct  $p_{\theta}(\mathbf{x}_{t-1} | \mathbf{x}_t)$  to approximate this probability and use a learning model  $\epsilon_{\theta}$  to predict the reverse noise  $\epsilon_t$  in the reverse diffusion process, similarly in DDPM. We can also demonstrate the simplified optimization objective in Theorem 1 for training  $\epsilon_{\theta}$  to learn an MDP.

**Theorem 1.** For the model  $\epsilon_{\theta}$  used to predict the reverse noise  $\epsilon_t$  in the reverse diffusion process of an MDP, its optimization objective at  $t$  for training can be simplified as

$$L_t^{\text{MDP}} = \mathbb{E}_{t \sim [1, T], \mathbf{x}_0, \epsilon_t} \left[ \|\epsilon_t - \epsilon_{\theta}(\sqrt{\bar{\alpha}_t} \mathbf{x}_0 + \sqrt{1 - \bar{\alpha}_t} \epsilon_t, t)\|^2 \right]. \quad (7)$$

The proof of Theorem 1 can be found in Appendix A.

### 4.2. Watermark Diffusion Process

We construct the watermark diffusion process based on the standard diffusion process, with the forward transition kernel as Equation. 1 for samples  $\mathbf{x}_0 \sim q(\mathbf{x})$ .

**Definition 2.** For samples  $\mathbf{x}_0 \sim q(\mathbf{x})$ , let  $\mathbf{x}_{1:T}$  denotes the states in a standard diffusion process with the forward transition kernel as Equation. 1. We define the process that has the state  $\tilde{\mathbf{x}}_t$  as

$$\tilde{\mathbf{x}}_t = \gamma_1 \mathbf{x}_t + (1 - \gamma_1) \mathbf{b}, \quad (8)$$

where constant  $\mathbf{b} \in \mathbb{R}^{\|\mathbf{x}_0\|}$  with  $\|\cdot\|$  as the dimension and  $\gamma_1 \in (0, 1)$ , for  $t \in \{0, \dots, T\}$  as a watermark diffusion process (a WDP).

The trigger  $\mathbf{b}$  drifts the mean of state distribution in the diffusion process. The states  $\tilde{\mathbf{x}}_{0:T}$  in a WDP shares the same reverse noise  $\epsilon$  with those in the standard diffusion process it is constructed on, since

$$\tilde{\mathbf{x}}_t = \gamma_1 \mathbf{x}_t + (1 - \gamma_1) \mathbf{b} = \gamma_1 \sqrt{\bar{\alpha}_t} \mathbf{x}_0 + \gamma_1 \sqrt{1 - \bar{\alpha}_t} \epsilon + (1 - \gamma_1) \mathbf{b}. \quad (9)$$

The shared reverse noise  $\epsilon_t$  leads us to the idea that we can recover data samples from the noisy distribution by obtaining it in the WDP for samples  $\mathbf{x}_0 \sim q(\mathbf{x})$  instead in its standard diffusion. The WDP can be used to learn a watermark distribution with the task distribution together using only one diffusion model without leaking the watermark during the task sampling process.

**Theorem 2.** *For samples  $\mathbf{x}_0 \sim q(\mathbf{x})$ , its WDP with Equation. 8 is exactly an MDP with the following configuration satisfied:*

$$\phi_t = \left( \frac{1}{\sqrt{\alpha_t}} - 1 \right) (1 - \gamma_1) \mathbf{b} \quad \text{and} \quad \eta = \gamma_1. \quad (10)$$

The proof of Theorem. 2 can be found in Appendix. A. It indicates that we can train the model  $\epsilon_\theta$  to learn a WDP using the objective in Theorem. 1 for the MDP. Until here, we have completed the theoretical foundations and analysis of our proposed watermarking method.

#### Algorithm 1 Watermark Embedding

```

1: Input: model  $\epsilon_\theta$ , training dataset  $\mathcal{D}_{\text{train}}$ , watermark dataset  $\mathcal{D}_{\text{wm}}$ , trigger  $\mathbf{b}$ , factor  $\gamma_1, \gamma_2$  and diffusion step  $T$ .
2: repeat
3:    $\mathbf{x}_0 \sim \mathcal{D}_{\text{train}}$ 
4:    $\mathbf{x}_0^w \sim \mathcal{D}_{\text{wm}}$ 
5:    $t \sim \text{Uniform}(\{1, \dots, T\})$ 
6:    $\epsilon, \epsilon^w \sim \mathcal{N}(\mathbf{0}, \mathbf{I})$ 
7:    $\mathbf{x}_t = \sqrt{\bar{\alpha}_t} \mathbf{x}_0 + \sqrt{1 - \bar{\alpha}_t} \epsilon$ 
8:    $\mathbf{x}_t^w = \sqrt{\bar{\alpha}_t} \mathbf{x}_0^w + \sqrt{1 - \bar{\alpha}_t} \epsilon^w$ 
9:   Take gradient descent step on
     $\nabla_\theta (\gamma_2 \|\epsilon - \epsilon_\theta(\mathbf{x}_t, t)\|^2 + \|\epsilon^w - \epsilon_\theta(\gamma_1 \mathbf{x}_t^w + (1 - \gamma_1) \mathbf{b}, t)\|^2)$ 
10: until converged

```

#### 4.3. Watermark Embedding

We embed the watermark by training the diffusion model to learn the task data through a standard diffusion process and the watermark data through a WDP together. The significance of this design is that task sampling does not generate samples in the watermark data distribution, which prevents the watermark from leaking and preserves the model's functionality. We demonstrate the embedding algorithm details in Algorithm. 1. Watermark embedding can be achieved by training from scratch or fine-tuning the pre-trained host model  $\epsilon_\theta^0$ . In each training iteration, we first

sample  $\mathbf{x}_0 \in \mathcal{D}_{\text{train}}$  and  $\mathbf{x}_0^w \in \mathcal{D}_{\text{wm}}$ . We then sample the noises  $\epsilon$  and  $\epsilon^w$  in this diffusion process separately from  $\mathcal{N}(\mathbf{0}, \mathbf{I})$  and the timestep  $t$  from  $\text{Uniform}(\{1, \dots, T\})$ . For the task sample  $\mathbf{x}_0$ , we calculate its state  $\mathbf{x}_t$  at  $t$  in its standard diffusion process. As for the watermark sample  $\mathbf{x}_0^w$ , we first calculate its state  $\mathbf{x}_t^w$  in the standard diffusion process. The corresponding state  $\tilde{\mathbf{x}}_t^w$  in the WDP can be constructed on  $\mathbf{x}_t^w$  as:

$$\tilde{\mathbf{x}}_t^w = \gamma_1 (\sqrt{\bar{\alpha}_t} \mathbf{x}_0^w + \sqrt{1 - \bar{\alpha}_t} \epsilon^w) + (1 - \gamma_1) \mathbf{b}. \quad (11)$$

Here  $\gamma_1$  is the trade-off factor for balancing the impact of the trigger  $\mathbf{b}$ . According to Theorem. 1 and Theorem. 2, we can obtain the training optimization objective for learning the standard process and WDP together, which is also the loss function for watermark embedding:

$$L_t^{\text{WDP}} = L_t^{\text{MDP}} = \gamma_2 \|\epsilon - \epsilon_\theta(\mathbf{x}_t, t)\|^2 + \|\epsilon^w - \epsilon_\theta(\tilde{\mathbf{x}}_t^w, t)\|^2, \quad (12)$$

where  $\gamma_2$  is a trade-off factor for balancing the standard and watermark diffusion processes.

#### Algorithm 2 Watermark Extraction

```

1: Input: model  $\epsilon_\theta$ , trigger  $\mathbf{b}$ , trigger factor  $\gamma_1$ , diffusion step  $T$ .
2:  $\mathbf{x}_T^w \sim \mathcal{N}(0, 1)$ 
3: for  $t = T, \dots, 1$  do
4:    $\mathbf{z} \sim \mathcal{N}(\mathbf{0}, \mathbf{I})$  if  $t > 1$  else  $\mathbf{z} = 0$ 
5:    $\mathbf{x}_{t-1}^w = \frac{1}{\sqrt{\alpha_t}} (\mathbf{x}_t^w - \frac{1 - \alpha_t}{\sqrt{1 - \alpha_t}} \epsilon_\theta(\gamma_1 \mathbf{x}_t^w + (1 - \gamma_1) \mathbf{b}, t)) + \sigma_t \mathbf{z}$ 
6: end for

```

#### 4.4. Watermark Extraction

Since the standard diffusion process and its constructed WDP share the same reverse noise, watermark extraction can be achieved through the standard reverse diffusion process using the reverse noise learned in the WDP. The detailed algorithm for watermark extraction is shown in Algorithm. 2. For a model  $\epsilon_\theta$ , given the trigger  $\mathbf{b}$  and trigger factor  $\gamma_1$ , we first sample  $\mathbf{x}_T^w$  from  $\mathcal{N}(0, 1)$ . We then compute the corresponding state  $\tilde{\mathbf{x}}_t^w$  in the WDP as  $\tilde{\mathbf{x}}_t^w = \gamma_1 \mathbf{x}_t^w + (1 - \gamma_1) \mathbf{b}$ . Finally, we take  $\tilde{\mathbf{x}}_t^w$  as one input to the diffusion model  $\epsilon_\theta$  for obtaining the shared reverse noise and the  $\mathbf{x}_{t-1}^w$ . To prevent leaking the watermark data during task sampling, trigger  $\mathbf{b}$  and trigger factor  $\gamma_1$  need to be chosen so there is enough divergence between the state distribution in the WDP and that in the standard process. We discuss the selection of suitable triggers and factors in Appendix. B.

#### 4.5. Watermark Verification

To verify the existence of the embedded watermark and given a conclusion about possible IP violations, we use a

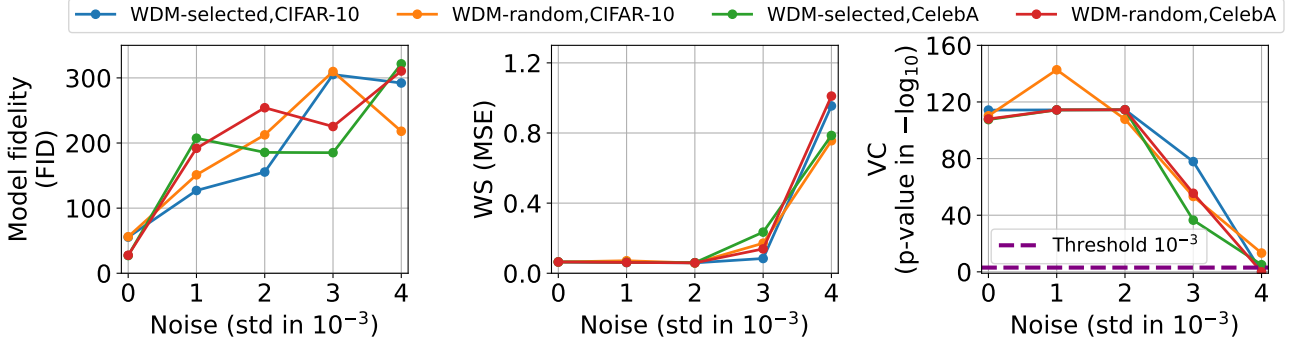


Figure 2: Results of model fidelity and watermark detectability for WDM against weight perturbation attacks. **Left:** The model fidelity in different WDM settings. **Middle:** The watermark similarity in different WDM settings. **Right:** The verification confidence in different WDM settings. The threshold line in the right figure represents the significance level  $10^{-3}$ .

two-step procedure, which contains watermark similarity comparison and hypothesis testing.

**Similarity Comparison.** We first measure the similarity  $d$  between the extracted watermark from model  $\epsilon_\theta$  and the embedded watermark from the model owner. For the setting that the watermark data distribution has a zero variance (watermark dataset contains only one sample), we use the Mean Square Error (MSE) between the embedded watermark sample  $\mathbf{a}$  and the extracted one  $\mathbf{a}_s$  to represent their similarity as  $d_s = d_{\text{MSE}}(\mathbf{a}, \mathbf{a}_s)$ . For the setting that the watermark dataset has a non-zero variance (contains multiple samples), we use the Fréchet Inception Distance (FID) score [36] between the embedded watermark data batch  $\mathbf{a}$  and the extracted batch  $\hat{\mathbf{a}}$  to measure their similarity as  $d_s = d_{\text{FID}}(\mathbf{a}, \mathbf{a}_s)$ . We also set the of watermark similarity from an independent model  $\epsilon_\theta^c$  without any watermark as  $d_c = d(\mathbf{a}, \mathbf{a}_c)$ . We denote the mean value of watermark similarity from the suspected model  $\epsilon_\theta^s$  as  $\mu_s = \bar{d}_s$ , and the mean value of that from  $\epsilon_\theta^c$  as  $\mu_c = \bar{d}_c$  for comparison.

**Hypothesis Testing.** After obtaining mean values of watermark similarity  $\mu_s$  and  $\mu_c$ , we use hypothesis testing to evaluate the confidence for whether or not the model is a stolen model. The test is about the mean values of two Gaussian distributions with different variances. Since smaller values indicate better similarities in both representations, we set the null hypothesis as  $H_0 : \mu_c \leq \mu_s$ , which indicates the suspected model is not stolen from the host. Its one-side alternative hypothesis is  $H_1 : \mu_c > \mu_s$ . The test either rejects  $H_0$  and gives the conclusion that the suspected model is stolen from the owner, or cannot reject it and gives the opposite conclusion.

## 5. Experiments

### 5.1. Experimental Settings

**Watermarking Configurations.** We conduct our experiments to evaluate the performance of our proposed WDM on two widely-used datasets, CIFAR-10 [37] and CelebA [38] as the benchmarks. FID score [36] between batches with 2000 samples is used as the evaluation metric for measuring the DM’s performance on task generation, which represents the model fidelity. Regarding the setting of watermark data distribution with a zero variance, we choose a specific image sample as shown in Fig. 1 as the target watermark data. In contrast, for the setting with a non-zero variance, we select the MNIST [39] as the target watermark dataset. The trigger can be a selected image with prior knowledge shown in Fig. 1, denoted as WDM-selected. We also test the setting that the trigger is a random image generated by a PRF given a secret key, denoted as WDM-random. We embed the watermark during training from scratch or fine-tuning all layers of the per-trained diffusion models using the loss in Equation. 12. The implementation of DDPM and our watermarking method is based on the work in [3]. Further details about the experiments and implementation can be found in Appendix. C. We conduct all experiments on AWS EC2 g4dn.4xlarge instances with NVIDIA T4 GPUs. All experiments about the FID scores are repeated 5 times and about MSE scores are repeated 100 times to obtain the mean values as results.

**Watermarking Robustness.** We evaluate the robustness of WDM against three model-transformation-based removing attacks: 1) model compression, 2) weight perturbation, and 3) model fine-tuning. We choose model quantization, which reduces the model’s size by quantizing the weights from 32-bit to 16-bit float numbers as the tested compression attack. We add random Gaussian noises with different standard

Embedding Settings	WDM-selected	WDM-random
Baseline(CIFAR-10)	$53.23 \pm 0.01$	$53.23 \pm 0.01$
TFS(CIFAR-10)	$55.44 \pm 0.07$	$61.72 \pm 0.19$
FT(CIFAR-10)	$56.09 \pm 0.39$	$65.40 \pm 0.53$
Baseline(CelebA)	$26.44 \pm 0.61$	$26.44 \pm 0.61$
TFS(CelebA)	$27.19 \pm 0.01$	$23.33 \pm 0.23$
FT(CelebA)	$27.67 \pm 0.24$	$23.10 \pm 0.08$

Table 1: The fidelity of watermarked DMs evaluated by the FID score in different configurations. Results are represented in the mean value with corresponding variance format. TFS and FT denote training from scratch and fine-tuning in embedding settings.

deviations to the model weights in each layer for the weight perturbation attack. We further evaluate the robustness of WDM against model fine-tuning by fine-tuning all layers of the watermarked DM.

## 5.2. Experimental Results

In this section, we present the experimental results and discussions about WDM with the three goals: model fidelity, watermark detectability, and watermark robustness. The ablation study with the hyperparameter trigger factor  $\gamma_1$  is also conducted. We only evaluate the setting where the watermark dataset contains only one sample in this section. The experiments under the setting where the watermark dataset contains multiple samples are presented in Appendix. D.

### 5.2.1. MODEL FIDELITY.

We present the fidelity of watermarked model with different embedding configurations in Table. 1. The degradation in fidelity caused by the WDM is not significant in both trigger settings. Comparing to embed the watermark through training-from-scratch, the fidelity degradation caused by fine-tuning is more unstable. The possible reason is that the fine-tuning based on the pre-trained DM is more difficulty to converge to the global optimal.

### 5.2.2. WATERMARK DETECTABILITY.

The watermark detectability results for the WDM with different configurations are presented in Table. 2. We can observe that the watermark similarity mean  $\mu_s$  of recovered target watermark data is significantly smaller than that from an independent model  $\mu_c$ , both in WDM-selected and WDM-random settings. The p-values of both configurations through training from scratch and fine-tuning are below the typical significance level of  $10^{-3}$  in the one-side hypothesis test. It indicates that the null hypothesis  $H_0$  can be rejected with a high enough significance, demonstrating the embedded watermark’s detectability.

Embedding Settings	WDM-selected		WDM-random	
	WS $\downarrow$ (MSE)	VC $\downarrow$ (p-value)	WS $\downarrow$ (MSE)	VC $\downarrow$ (p-value)
Baseline(CIFAR-10)	0.92918	$10^{-1}$	1.03738	$10^{-1}$
TFS(CIFAR-10)	0.06428	$10^{-198}$	0.06429	$10^{-185}$
FT(CIFAR-10)	0.06413	$10^{-198}$	0.06379	$10^{-185}$
Baseline(CelebA)	0.92790	$10^{-1}$	1.04821	$10^{-1}$
TFS(CelebA)	0.06461	$10^{-190}$	0.06448	$10^{-186}$
FT(CelebA)	0.06391	$10^{-190}$	0.06399	$10^{-186}$

Table 2: Results for the detectability of the WDM in different configurations. We denote the watermark similarity and verification confidence as WS and VC separately.

Embedding Settings	WDM-selected		WDM-random	
	$\Delta$ WS $\downarrow$ (MSE)	VC $\downarrow$ (p-value)	$\Delta$ WS $\downarrow$ (MSE)	VC $\downarrow$ (p-value)
TFS(CIFAR-10)	$10^{-4}$	$10^{-115}$	$10^{-4}$	$10^{-108}$
FT(CIFAR-10)	$10^{-4}$	$10^{-115}$	$10^{-4}$	$10^{-108}$
TFS(CelebA)	$10^{-6}$	$10^{-111}$	$10^{-6}$	$10^{-109}$
FT(CelebA)	$10^{-6}$	$10^{-111}$	$10^{-6}$	$10^{-109}$

Table 3: Results of watermark similarities and verification confidence for WDM against model compression attacks in different configurations.

### 5.2.3. WATERMARK ROBUSTNESS

**Model Compression.** The results of the WDM against model compression attacks are presented in Table. 3. It can be observed that the watermark similarities from the compressed watermarked DMs have no significant degradation compared with those from the watermarked DMs. The p-values are still below the significance level, which indicates the robustness of the WDM against the model compression attack in our settings.

**Weight Perturbation.** We demonstrate the model fidelity and watermark detectability of the WDM against weight perturbation attacks in Figure. 2. The standard deviation (std) of Gaussian noises added to model weights ranges from  $1 \times 10^{-3}$  to  $4 \times 10^{-3}$ . We can observe a significant decrease in model fidelity as the std of noises added increases. However, the watermark still can be detected and verified as the std is smaller than  $3 \times 10^{-3}$ . These results indicate that our proposed WDM is robust against model weight perturbation in our settings.

**Model Fine-tuning.** We demonstrate the results of the fidelity and watermark similarities along with the fine-tuning epoch in Figure. 3. For both CIFAR-10 and CelebA task datasets, it can be observed that WDM-selected is still effective after fine-tuning. However, WDM-random is no longer effective after fine-tuning half of the largest epoch number, which indicates that WDM-selected is more resistant to model fine-tuning attacks. The reason is that the

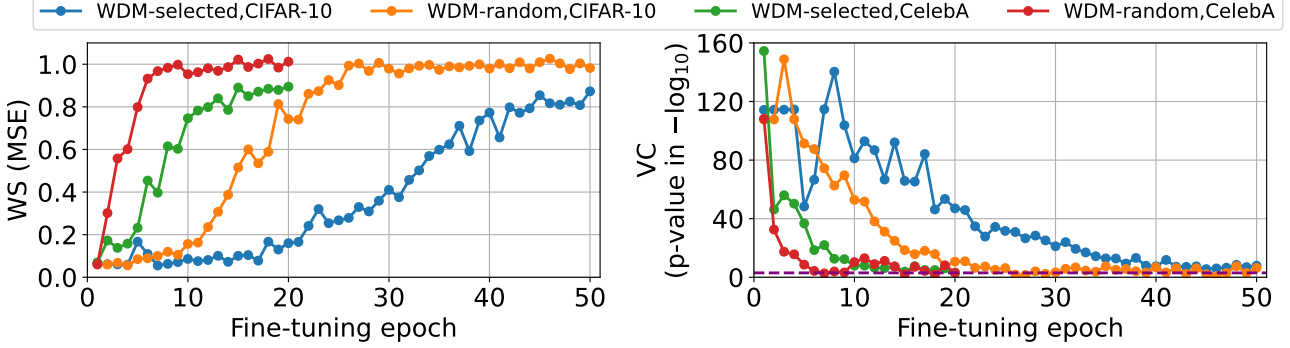


Figure 3: Results of watermark detectability for WDM against model fine-tuning attacks. **Left:** The watermark similarity in different WDM settings. **Right:** The verification confidence in different WDM settings. The threshold line in the right figure represents significance level  $10^{-3}$ .

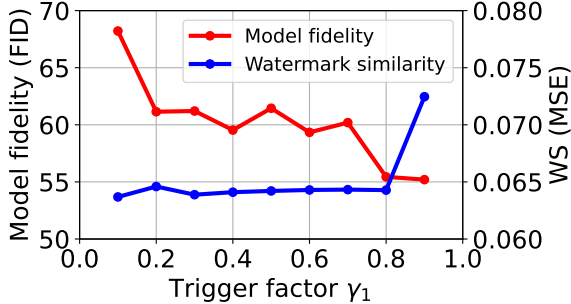


Figure 4: Results of model fidelity and watermark detectability of WDM-selected with the trigger factor  $\gamma_1$  training on CIFAR-10 dataset.

state distribution in the WDP using the selected trigger has a larger distribution divergence than that of the randomly generated trigger, making it harder to remove the embedded watermark by fine-tuning.

#### 5.2.4. IMPACT OF TRIGGER FACTOR $\gamma_1$

We conduct an ablation study on the fidelity and detectability of the WDM against the trigger factor  $\gamma_1$ , with the watermark trigger as selected and dataset as CIFAR-10. The experiment results shown in Figure 4 indicates that the fidelity and detectability of WDM are not significantly influenced by the factor  $\gamma_1$ . Moreover, we can observe a trend that fidelity of the watermarked DM increases with a larger  $\gamma_1$  value while the detectability decreases. This is because a larger  $\gamma_1$  reduces the distribution divergence between the state in WDP and that in a standard diffusion process for the watermark data, making it harder to embed the watermark.

## 6. Conclusions

In this paper, we propose a complete watermarking method WDM for diffusion models, including watermark embed-

ding, extraction, and verification. We construct a watermark diffusion process for the watermark data based on its standard diffusion process. By training the diffusion model to learn a standard diffusion process for task data and a WDP for the watermark data, we can embed the watermark into DMs. Watermark extraction is processed by sampling the watermark data using the shared reverse noise learned by the WDP. The extracted watermark can be verified by comparing the similarity and performing the hypothesis test, which gives the conclusion about the model IP violation. We provide the theoretical foundations and analysis to WDM and validate its performance through our experiments. Overall, the proposed method can achieve the goals of model fidelity, watermark detectability, and watermark robustness. Introducing this new approach has provided a powerful tool for protecting intellectual property in diffusion models.

## References

- [1] J. Sohl-Dickstein, E. A. Weiss, N. Maheswaranathan, and S. Ganguli, “Deep unsupervised learning using nonequilibrium thermodynamics,” in *Proceedings of the 32nd International Conference on Machine Learning, ICML 2015, Lille, France, 6-11 July 2015* (F. R. Bach and D. M. Blei, eds.), vol. 37 of *JMLR Workshop and Conference Proceedings*, pp. 2256–2265, JMLR.org, 2015.
- [2] J. Ho, A. Jain, and P. Abbeel, “Denoising diffusion probabilistic models,” in *Advances in Neural Information Processing Systems 33: Annual Conference on Neural Information Processing Systems 2020, NeurIPS 2020, December 6-12, 2020, virtual* (H. Larochelle, M. Ranzato, R. Hadsell, M. Balcan, and H. Lin, eds.), 2020.
- [3] A. Q. Nichol and P. Dhariwal, “Improved denoising diffusion probabilistic models,” in *Proceedings of the*

*38th International Conference on Machine Learning, ICML 2021, 18-24 July 2021, Virtual Event* (M. Meila and T. Zhang, eds.), vol. 139 of *Proceedings of Machine Learning Research*, pp. 8162–8171, PMLR, 2021.

[4] P. Dhariwal and A. Q. Nichol, “Diffusion models beat gans on image synthesis,” in *Advances in Neural Information Processing Systems 34: Annual Conference on Neural Information Processing Systems 2021, NeurIPS 2021, December 6-14, 2021, virtual* (M. Ranzato, A. Beygelzimer, Y. N. Dauphin, P. Liang, and J. W. Vaughan, eds.), pp. 8780–8794, 2021.

[5] A. Brock, J. Donahue, and K. Simonyan, “Large scale GAN training for high fidelity natural image synthesis,” in *7th International Conference on Learning Representations, ICLR 2019, New Orleans, LA, USA, May 6-9, 2019*, OpenReview.net, 2019.

[6] I. J. Goodfellow, J. Pouget-Abadie, M. Mirza, B. Xu, D. Warde-Farley, S. Ozair, A. C. Courville, and Y. Bengio, “Generative adversarial networks,” *Commun. ACM*, vol. 63, no. 11, pp. 139–144, 2020.

[7] D. P. Kingma and M. Welling, “Auto-encoding variational bayes,” in *2nd International Conference on Learning Representations, ICLR 2014, Banff, AB, Canada, April 14-16, 2014, Conference Track Proceedings* (Y. Bengio and Y. LeCun, eds.), 2014.

[8] A. van den Oord, O. Vinyals, and K. Kavukcuoglu, “Neural discrete representation learning,” in *Advances in Neural Information Processing Systems 30: Annual Conference on Neural Information Processing Systems 2017, December 4-9, 2017, Long Beach, CA, USA* (I. Guyon, U. von Luxburg, S. Bengio, H. M. Wallach, R. Fergus, S. V. N. Vishwanathan, and R. Garnett, eds.), pp. 6306–6315, 2017.

[9] R. Rombach, A. Blattmann, D. Lorenz, P. Esser, and B. Ommer, “High-resolution image synthesis with latent diffusion models,” in *IEEE/CVF Conference on Computer Vision and Pattern Recognition, CVPR 2022, New Orleans, LA, USA, June 18-24, 2022*, pp. 10674–10685, IEEE, 2022.

[10] A. Ramesh, M. Pavlov, G. Goh, S. Gray, C. Voss, A. Radford, M. Chen, and I. Sutskever, “Zero-shot text-to-image generation,” in *Proceedings of the 38th International Conference on Machine Learning, ICML 2021, 18-24 July 2021, Virtual Event* (M. Meila and T. Zhang, eds.), vol. 139 of *Proceedings of Machine Learning Research*, pp. 8821–8831, PMLR, 2021.

[11] Y. Li, H. Wang, and M. Barni, “A survey of deep neural network watermarking techniques,” *Neurocomputing*, vol. 461, pp. 171–193, 2021.

[12] S. Peng, Y. Chen, J. Xu, Z. Chen, C. Wang, and X. Jia, “Intellectual property protection of dnn models,” *World Wide Web*, pp. 1–35, 2022.

[13] Y. Uchida, Y. Nagai, S. Sakazawa, and S. Satoh, “Embedding watermarks into deep neural networks,” in *Proceedings of the 2017 ACM on International Conference on Multimedia Retrieval, ICMR 2017, Bucharest, Romania, June 6-9, 2017* (B. Ionescu, N. Sebe, J. Feng, M. A. Larson, R. Lienhart, and C. Snoek, eds.), pp. 269–277, ACM, 2017.

[14] H. Chen, B. D. Rouhani, C. Fu, J. Zhao, and F. Koushanfar, “Deepmarks: A secure fingerprinting framework for digital rights management of deep learning models,” in *Proceedings of the 2019 on International Conference on Multimedia Retrieval, ICMR 2019, Ottawa, ON, Canada, June 10-13, 2019* (A. El-Saddik, A. D. Bimbo, Z. Zhang, A. G. Hauptmann, K. S. Candan, M. Bertini, L. Xie, and X. Wei, eds.), pp. 105–113, ACM, 2019.

[15] T. Wang and F. Kerschbaum, “RIGA: covert and robust white-box watermarking of deep neural networks,” in *WWW ’21: The Web Conference 2021, Virtual Event / Ljubljana, Slovenia, April 19-23, 2021* (J. Leskovec, M. Grobelnik, M. Najork, J. Tang, and L. Zia, eds.), pp. 993–1004, ACM / IW3C2, 2021.

[16] H. Liu, Z. Weng, and Y. Zhu, “Watermarking deep neural networks with greedy residuals,” in *Proceedings of the 38th International Conference on Machine Learning, ICML 2021, 18-24 July 2021, Virtual Event* (M. Meila and T. Zhang, eds.), vol. 139 of *Proceedings of Machine Learning Research*, pp. 6978–6988, PMLR, 2021.

[17] E. L. Merrer, P. Pérez, and G. Trédan, “Adversarial frontier stitching for remote neural network watermarking,” *Neural Comput. Appl.*, vol. 32, no. 13, pp. 9233–9244, 2020.

[18] P. Yang, Y. Lao, and P. Li, “Robust watermarking for deep neural networks via bi-level optimization,” in *2021 IEEE/CVF International Conference on Computer Vision, ICCV 2021, Montreal, QC, Canada, October 10-17, 2021*, pp. 14821–14830, IEEE, 2021.

[19] Y. Adi, C. Baum, M. Cissé, B. Pinkas, and J. Keshet, “Turning your weakness into a strength: Watermarking deep neural networks by backdooring,” in *27th USENIX Security Symposium, USENIX Security 2018, Baltimore, MD, USA, August 15-17, 2018* (W. Enck and A. P. Felt, eds.), pp. 1615–1631, USENIX Association, 2018.

[20] J. Zhang, Z. Gu, J. Jang, H. Wu, M. P. Stoecklin, H. Huang, and I. M. Molloy, “Protecting intellectual property of deep neural networks with watermarking,” in *Proceedings of the 2018 on Asia Conference on Computer and Communications Security, AsiaCCS 2018, Incheon, Republic of Korea, June 04-08, 2018* (J. Kim, G. Ahn, S. Kim, Y. Kim, J. López, and T. Kim, eds.), pp. 159–172, ACM, 2018.

[21] J. Guo and M. Potkonjak, “Watermarking deep neural networks for embedded systems,” in *Proceedings of the International Conference on Computer-Aided Design, ICCAD 2018, San Diego, CA, USA, November 05-08, 2018* (I. Bahar, ed.), p. 133, ACM, 2018.

[22] Z. Li, C. Hu, Y. Zhang, and S. Guo, “How to prove your model belongs to you: a blind-watermark based framework to protect intellectual property of DNN,” in *Proceedings of the 35th Annual Computer Security Applications Conference, ACSAC 2019, San Juan, PR, USA, December 09-13, 2019* (D. Balenson, ed.), pp. 126–137, ACM, 2019.

[23] B. D. Rouhani, H. Chen, and F. Koushanfar, “Deep-signs: An end-to-end watermarking framework for ownership protection of deep neural networks,” in *Proceedings of the Twenty-Fourth International Conference on Architectural Support for Programming Languages and Operating Systems, ASPLOS 2019, Providence, RI, USA, April 13-17, 2019* (I. Bahar, M. Herlihy, E. Witchel, and A. R. Lebeck, eds.), pp. 485–497, ACM, 2019.

[24] R. Namba and J. Sakuma, “Robust watermarking of neural network with exponential weighting,” in *Proceedings of the 2019 ACM Asia Conference on Computer and Communications Security, AsiaCCS 2019, Auckland, New Zealand, July 09-12, 2019* (S. D. Galbraith, G. Russello, W. Susilo, D. Gollmann, E. Kirda, and Z. Liang, eds.), pp. 228–240, ACM, 2019.

[25] H. Jia, C. A. Choquette-Choo, V. Chandrasekaran, and N. Papernot, “Entangled watermarks as a defense against model extraction,” in *30th USENIX Security Symposium, USENIX Security 2021, August 11-13, 2021* (M. Bailey and R. Greenstadt, eds.), pp. 1937–1954, USENIX Association, 2021.

[26] S. Szyller, B. G. Atli, S. Marchal, and N. Asokan, “DAWN: dynamic adversarial watermarking of neural networks,” in *MM '21: ACM Multimedia Conference, Virtual Event, China, October 20 - 24, 2021* (H. T. Shen, Y. Zhuang, J. R. Smith, Y. Yang, P. César, F. Metze, and B. Prabhakaran, eds.), pp. 4417–4425, ACM, 2021.

[27] D. S. Ong, C. S. Chan, K. W. Ng, L. Fan, and Q. Yang, “Protecting intellectual property of generative adversarial networks from ambiguity attacks,” in *IEEE Conference on Computer Vision and Pattern Recognition, CVPR 2021, virtual, June 19-25, 2021*, pp. 3630–3639, Computer Vision Foundation / IEEE, 2021.

[28] Y. Zhao, T. Pang, C. Du, X. Yang, N. Cheung, and M. Lin, “A recipe for watermarking diffusion models,” *CoRR*, vol. abs/2303.10137, 2023.

[29] J. Fei, Z. Xia, B. Tondi, and M. Barni, “Supervised GAN watermarking for intellectual property protection,” in *IEEE International Workshop on Information Forensics and Security, WIFS 2022, Shanghai, China, December 12-16, 2022*, pp. 1–6, IEEE, 2022.

[30] N. Yu, V. Skripniuk, S. Abdehnabi, and M. Fritz, “Artificial fingerprinting for generative models: Rooting deepfake attribution in training data,” in *2021 IEEE/CVF International Conference on Computer Vision, ICCV 2021, Montreal, QC, Canada, October 10-17, 2021*, pp. 14428–14437, IEEE, 2021.

[31] Y. Song, J. Sohl-Dickstein, D. P. Kingma, A. Kumar, S. Ermon, and B. Poole, “Score-based generative modeling through stochastic differential equations,” in *9th International Conference on Learning Representations, ICLR 2021, Virtual Event, Austria, May 3-7, 2021*, OpenReview.net, 2021.

[32] Y. Song and S. Ermon, “Generative modeling by estimating gradients of the data distribution,” in *Advances in Neural Information Processing Systems 32: Annual Conference on Neural Information Processing Systems 2019, NeurIPS 2019, December 8-14, 2019, Vancouver, BC, Canada* (H. M. Wallach, H. Larochelle, A. Beygelzimer, F. d’Alché-Buc, E. B. Fox, and R. Garnett, eds.), pp. 11895–11907, 2019.

[33] J. Song, C. Meng, and S. Ermon, “Denoising diffusion implicit models,” in *9th International Conference on Learning Representations, ICLR 2021, Virtual Event, Austria, May 3-7, 2021*, OpenReview.net, 2021.

[34] A. Vahdat, K. Kreis, and J. Kautz, “Score-based generative modeling in latent space,” in *Advances in Neural Information Processing Systems 34: Annual Conference on Neural Information Processing Systems 2021, NeurIPS 2021, December 6-14, 2021, virtual* (M. Ranzato, A. Beygelzimer, Y. N. Dauphin, P. Liang, and J. W. Vaughan, eds.), pp. 11287–11302, 2021.

[35] S. Chou, P. Chen, and T. Ho, “How to backdoor diffusion models?,” *CoRR*, vol. abs/2212.05400, 2022.

- [36] M. Heusel, H. Ramsauer, T. Unterthiner, B. Nessler, and S. Hochreiter, “Gans trained by a two time-scale update rule converge to a local nash equilibrium,” in *Advances in Neural Information Processing Systems 30: Annual Conference on Neural Information Processing Systems 2017, December 4-9, 2017, Long Beach, CA, USA* (I. Guyon, U. von Luxburg, S. Bengio, H. M. Wallach, R. Fergus, S. V. N. Vishwanathan, and R. Garnett, eds.), pp. 6626–6637, 2017.
- [37] A. Krizhevsky, G. Hinton, *et al.*, “Learning multiple layers of features from tiny images,” 2009.
- [38] Z. Liu, P. Luo, X. Wang, and X. Tang, “Deep learning face attributes in the wild,” in *Proceedings of International Conference on Computer Vision (ICCV)*, December 2015.
- [39] Y. LeCun, L. D. Jackel, L. Bottou, C. Cortes, J. S. Denker, H. Drucker, I. Guyon, U. A. Muller, E. Sackinger, P. Simard, *et al.*, “Learning algorithms for classification: A comparison on handwritten digit recognition,” *Neural networks: the statistical mechanics perspective*, vol. 261, no. 276, p. 2, 1995.

## A. Theoretical Analysis for the MDP and WDP

### A.1. Proof of Theorem. 1

In this part, we first prove the Theorem 1. We know that for  $t \in \{1, \dots, T\}$ , the transition kernel of an MDP is

$$q(\mathbf{x}_t | \mathbf{x}_{t-1}) = \mathcal{N}(\mathbf{x}_t; \sqrt{\alpha_t} \mathbf{x}_{t-1} + \sqrt{\alpha_t} \boldsymbol{\phi}_t, \eta^2(1 - \alpha_t) \mathbf{I}) \quad (13)$$

*Proof.* Using the re-parameterization trick, we can get

$$\begin{aligned} \mathbf{x}_t &= \sqrt{\alpha_t} \mathbf{x}_{t-1} + \sqrt{\alpha_t} \boldsymbol{\phi}_t + \eta \sqrt{1 - \alpha_t} \boldsymbol{\epsilon}_t \\ &= \sqrt{\alpha_t} (\sqrt{\alpha_{t-1}} \mathbf{x}_{t-2} + \sqrt{\alpha_{t-1}} \boldsymbol{\phi}_{t-1} + \eta \sqrt{1 - \alpha_{t-1}} \boldsymbol{\epsilon}_{t-1}) + \sqrt{\alpha_t} \boldsymbol{\phi}_t + \eta \sqrt{1 - \alpha_t} \boldsymbol{\epsilon}_t \\ &= \sqrt{\alpha_t \alpha_{t-1}} \mathbf{x}_{t-2} + (\sqrt{\alpha_t} \boldsymbol{\phi}_t + \sqrt{\alpha_t \alpha_{t-1}} \boldsymbol{\phi}_{t-1}) + \eta (\sqrt{\alpha_t(1 - \alpha_{t-1})} \boldsymbol{\epsilon}_{t-1} + \sqrt{1 - \alpha_t} \boldsymbol{\epsilon}_t) \\ &= \sqrt{\alpha_t \alpha_{t-1}} \mathbf{x}_{t-2} + (\sqrt{\alpha_t} \boldsymbol{\phi}_t + \sqrt{\alpha_t \alpha_{t-1}} \boldsymbol{\phi}_{t-1}) + \eta \sqrt{1 - \alpha_t \alpha_{t-1}} \boldsymbol{\epsilon}_{t,t-1} \\ &= \sqrt{\bar{\alpha}_t} \mathbf{x}_0 + \sum_{i=1}^t (\sqrt{\prod_{j=t+1-i}^t \alpha_j} \boldsymbol{\phi}_{t+1-i}) + \eta \sqrt{1 - \bar{\alpha}_t} \hat{\boldsymbol{\epsilon}}, \end{aligned} \quad (14)$$

where  $\boldsymbol{\epsilon}_{t,t-1}, \hat{\boldsymbol{\epsilon}} \sim \mathcal{N}(0, 1)$ . We can find the distribution of  $q(\mathbf{x}_t | \mathbf{x}_0)$  is still a Gaussian distribution and can be implicitly expressed as

$$q(\mathbf{x}_t | \mathbf{x}_0) \sim \mathcal{N}(\mathbf{x}_0; \sqrt{\bar{\alpha}_t} \mathbf{x}_0 + \tilde{\boldsymbol{\phi}}_t, \eta^2(1 - \bar{\alpha}_t) \mathbf{I}), \quad (15)$$

where

$$\tilde{\boldsymbol{\phi}}_t = \sum_{i=1}^t (\sqrt{\prod_{j=t+1-i}^t \alpha_j} \boldsymbol{\phi}_{t+1-i}) \quad (16)$$

The transition kernel conditioned on  $\mathbf{x}_0$  in the reverse diffusion process of an MDP can be represented as

$$q(\mathbf{x}_{t-1} | \mathbf{x}_t, \mathbf{x}_0) = \mathcal{N}(\mathbf{x}_{t-1}; \tilde{\boldsymbol{\mu}}_t(\mathbf{x}_t, \mathbf{x}_0), \tilde{\sigma}_t \mathbf{I}). \quad (17)$$

Using the Bayes rule, we can get

$$\begin{aligned} q(\mathbf{x}_{t-1} | \mathbf{x}_t, \mathbf{x}_0) &= q(\mathbf{x}_t | \mathbf{x}_{t-1}, \mathbf{x}_0) \frac{q(\mathbf{x}_{t-1} | \mathbf{x}_0)}{q(\mathbf{x}_t | \mathbf{x}_0)} \\ &\propto \exp \left( -\frac{1}{2} \left( \frac{(\mathbf{x}_t - \sqrt{\alpha_t} \mathbf{x}_{t-1} - \sqrt{\alpha_t} \boldsymbol{\phi}_t)^2}{\eta^2(1 - \alpha_t)} + \frac{(\mathbf{x}_{t-1} - \sqrt{\bar{\alpha}_{t-1}} \mathbf{x}_0 - \tilde{\boldsymbol{\phi}}_{t-1})^2}{\eta^2(1 - \bar{\alpha}_{t-1})} - \frac{(\mathbf{x}_t - \sqrt{\bar{\alpha}_t} \mathbf{x}_0 - \tilde{\boldsymbol{\phi}}_t)^2}{\eta^2(1 - \bar{\alpha}_t)} \right) \right) \\ &= \exp \left( -\frac{1}{2\eta^2} \left( \frac{(\mathbf{x}_t - \sqrt{\alpha_t} \boldsymbol{\phi}_t)^2 - 2\sqrt{\alpha_t}(\mathbf{x}_t - \sqrt{\alpha_t} \boldsymbol{\phi}_t)\mathbf{x}_{t-1} + \alpha_t \mathbf{x}_{t-1}^2}{1 - \alpha_t} \right. \right. \\ &\quad \left. \left. + \frac{\mathbf{x}_{t-1}^2 - 2(\sqrt{\bar{\alpha}_{t-1}} \mathbf{x}_0 + \tilde{\boldsymbol{\phi}}_{t-1})\mathbf{x}_{t-1} + (\sqrt{\bar{\alpha}_{t-1}} \mathbf{x}_0 + \tilde{\boldsymbol{\phi}}_t)^2}{1 - \bar{\alpha}_{t-1}} - \frac{(\mathbf{x}_t - \sqrt{\bar{\alpha}_t} \mathbf{x}_0 - \tilde{\boldsymbol{\phi}}_t)^2}{1 - \bar{\alpha}_t} \right) \right) \\ &= \exp \left( -\frac{1}{2} \left( \frac{1}{\eta^2} \left( \frac{\alpha_t}{1 - \alpha_t} + \frac{1}{1 - \bar{\alpha}_{t-1}} \right) \mathbf{x}_{t-1}^2 - \frac{2}{\eta^2} \left( \frac{\sqrt{\alpha_t}(\mathbf{x}_t - \sqrt{\alpha_t} \boldsymbol{\phi}_t)}{1 - \alpha_t} \right. \right. \right. \\ &\quad \left. \left. \left. + \frac{\sqrt{\bar{\alpha}_{t-1}} \mathbf{x}_0 + \tilde{\boldsymbol{\phi}}_{t-1}}{1 - \bar{\alpha}_{t-1}} \mathbf{x}_{t-1} + C(\mathbf{x}_t, \mathbf{x}_0) \right) \right) \right) \end{aligned}$$

We can get the mean and variance of this Gaussian distribution as

$$\tilde{\sigma}_t = \frac{1}{\frac{1}{\eta^2} \left( \frac{\alpha_t}{1 - \alpha_t} + \frac{1}{1 - \bar{\alpha}_{t-1}} \right)} = \frac{\eta^2(1 - \bar{\alpha}_{t-1})(1 - \alpha_t)}{1 - \bar{\alpha}_t}, \quad (18)$$

and

$$\tilde{\mu}_t(\mathbf{x}_t, \mathbf{x}_0) = \frac{1}{\eta^2} \left( \frac{\sqrt{\alpha_t}(\mathbf{x}_t - \sqrt{\alpha_t} \phi_t)}{1 - \alpha_t} + \frac{\sqrt{\bar{\alpha}_{t-1}} \mathbf{x}_0 + \tilde{\phi}_{t-1}}{1 - \bar{\alpha}_{t-1}} \right) / \frac{1}{\eta^2} \left( \frac{\alpha_t}{1 - \alpha_t} + \frac{1}{1 - \bar{\alpha}_{t-1}} \right) \quad (19)$$

$$= \frac{\sqrt{\alpha_t}(1 - \bar{\alpha}_{t-1})}{1 - \bar{\alpha}_t} \mathbf{x}_t + \frac{\sqrt{\bar{\alpha}_{t-1}}(1 - \alpha_t)}{1 - \bar{\alpha}_t} \mathbf{x}_0 + \frac{\bar{\alpha}_t - \alpha_t}{1 - \bar{\alpha}_t} \phi_t + \frac{1 - \alpha_t}{1 - \bar{\alpha}_t} \tilde{\phi}_{t-1}. \quad (20)$$

By replacing  $\mathbf{x}_0$  above with  $\mathbf{x}_0 = \frac{1}{\sqrt{\bar{\alpha}_t}}(\mathbf{x}_t - \tilde{\phi}_t - \eta\sqrt{1 - \bar{\alpha}_t}\epsilon_t)$ , we can get

$$\tilde{\mu}_t = \frac{1}{\sqrt{\alpha_t}} \left( \mathbf{x}_t - \eta \frac{1 - \alpha_t}{\sqrt{1 - \bar{\alpha}_t}} \epsilon_t \right) + C_t, \quad (21)$$

where  $C_t$  is a constant term. Following the same simplification in DDPM [2], we can get the training objective as

$$L_t^{\text{MDP}} = \mathbb{E}_{t \sim [1, T], \mathbf{x}_0, \epsilon_t} \left[ \|\epsilon_t - \epsilon_\theta(\mathbf{x}_t, t)\|^2 \right] \quad (22)$$

$$= \mathbb{E}_{t \sim [1, T], \mathbf{x}_0, \epsilon_t} \left[ \|\epsilon_t - \epsilon_\theta(\sqrt{\bar{\alpha}_t} \mathbf{x}_0 + \sqrt{1 - \bar{\alpha}_t} \epsilon_t, t)\|^2 \right] \quad (23)$$

Theorem. 1 is proved. The simplified loss is the same as the one in DDPM.  $\square$

## A.2. Proof of Theorem. 2

*Proof.* By replacing the  $\mathbf{x}_t$  in Equation. 8 using Equation. 2, we can get

$$\tilde{\mathbf{x}}_t = \gamma_1 \mathbf{x}_t + (1 - \gamma_1) \mathbf{b} \quad (24)$$

$$= \gamma_1 (\sqrt{\bar{\alpha}_t} \mathbf{x}_0 + \sqrt{1 - \bar{\alpha}_t} \epsilon) + (1 - \gamma_1) \mathbf{b}. \quad (25)$$

Then we replace the  $\mathbf{x}_0$  using Equation 2 to get

$$\tilde{\mathbf{x}}_t = \gamma_1 (\sqrt{\bar{\alpha}_t} \mathbf{x}_0 + \sqrt{1 - \bar{\alpha}_t} \epsilon) + (1 - \gamma_1) \mathbf{b} \quad (26)$$

$$= \gamma_1 \sqrt{\bar{\alpha}_t} \left( \frac{\tilde{\mathbf{x}}_0 - (1 - \gamma_1) \mathbf{b}}{\gamma_1} \right) + \gamma_1 \sqrt{1 - \bar{\alpha}_t} \epsilon + (1 - \gamma_1) \mathbf{b} \quad (27)$$

$$= \sqrt{\bar{\alpha}_t} \tilde{\mathbf{x}}_0 + (1 - \sqrt{\bar{\alpha}_t})(1 - \gamma_1) \mathbf{b} + \gamma_1 \sqrt{1 - \bar{\alpha}_t} \epsilon. \quad (28)$$

Compare  $q(\tilde{\mathbf{x}}_t | \tilde{\mathbf{x}}_0)$  to the diffusion process with the modified Gaussian kernel, we can get they are the same if the configurations satisfy

$$\tilde{\phi}_t = (1 - \sqrt{\bar{\alpha}_t})(1 - \gamma_1) \mathbf{b} \quad (29)$$

and

$$\eta = \gamma_1. \quad (30)$$

Based on Equation. 16, we can represent  $\phi_t$  as

$$\phi_t = \frac{\tilde{\phi}_t}{\sqrt{\alpha_t}} - \tilde{\phi}_{t-1} = \left( \frac{1}{\sqrt{\alpha_t}} - 1 \right) (1 - \gamma_1) \mathbf{b} \quad (31)$$

Then we complete the proof.  $\square$

## B. Selection of Triggers and Trigger Factors

To ensure the watermark data has no leakage during the standard diffusion process, the trigger  $\mathbf{b}$  and trigger factor  $\gamma_1$  need to be selected in such a way that there is a sufficient divergence between the WDP and the standard diffusion process. We denote the probability distribution of states in recovering the watermark data through the standard reverse diffusion process as  $q(\mathbf{x}_{t-1}^w | \mathbf{x}_t^w, \mathbf{x}_0^w)$ , and that of the states in learned reverse process of the WDP as  $q(\tilde{\mathbf{x}}_{t-1}^w | \tilde{\mathbf{x}}_t^w, \tilde{\mathbf{x}}_0^w)$ . We need to ensure their divergence is sufficient enough so that the standard reverse process does not recover the watermark data through  $q(\mathbf{x}_{t-1}^w | \mathbf{x}_t^w, \mathbf{x}_0^w)$ . If there is no divergence between these two distributions, as in the case when  $\gamma_1 = 1$  or  $\mathbf{b} = \mathbf{0}$ , the WDP

becomes the standard diffusion process for the watermark data, which can result in the watermark leakage. By replacing the  $\tilde{\phi}_t$  and  $\eta$  in Equation. 21 with Equation. 10, we can obtain the mean value of  $q(\tilde{\mathbf{x}}_{t-1}^w | \tilde{\mathbf{x}}_t^w, \tilde{\mathbf{x}}_0^w)$  in the WDP as follows:

$$\tilde{\mu}_t(\tilde{\mathbf{x}}_t^w) = \frac{1}{\sqrt{\alpha_t}} \left( \tilde{\mathbf{x}}_t^w - \gamma_1 \frac{1 - \alpha_t}{\sqrt{1 - \bar{\alpha}_t}} \epsilon_t \right) + (1 - \frac{1}{\sqrt{\alpha_t}})(1 - \gamma_1)\mathbf{b}. \quad (32)$$

Since the mean value of  $\mathbf{x}_{t-1}^w$  in the standard reverse process is as follows:

$$\mu_t(\mathbf{x}_t^w) = \frac{1}{\sqrt{\alpha_t}} \left( \mathbf{x}_t^w - \frac{1 - \alpha_t}{\sqrt{1 - \bar{\alpha}_t}} \epsilon_t \right), \quad (33)$$

we can present their difference as follows:

$$\tilde{\mu}_t - \mu_t = \frac{1}{\sqrt{\alpha_t}} \left( \mathbf{x}_t^w - \frac{1 - \alpha_t}{\sqrt{1 - \bar{\alpha}_t}} \epsilon_t - \mathbf{b} \right) (1 - \gamma_1). \quad (34)$$

We observe that we can choose a relatively small  $\gamma_1$  to increase the divergence between these two distributions. Furthermore, the trigger  $\mathbf{b}$  needs to be chosen from a distribution that is different from the states involved in the standard diffusion process for the task data. In practice, we can choose an Out-Of-Distribution (OOD) sample from the task data, such as a selected image with ownership information as the trigger, as we have done in our WDP-selected.

## C. Experiment Implementation Details

### C.1. Network Implementation and Parameters

We have implemented DDPMs following the approach presented in [3]. To build the backbone of the diffusion model, we use the UNet architecture introduced by Ho et al. in [2]. The UNet model employs stacks of residual layers and downsampling/upsampling convolutions. The timestep is encoded using positional encoding and add it to each residual block using a global attention layer with multiple heads. In our experiments, we set the global attention with 4 heads and a resolution of  $16 \times 16$ . We also set the base channels to 128, and include 3 residual blocks per resolution. The process steps in both standard diffusion process and the WDP is set to 1000.

### C.2. Training Parameters

During the model training, we set the image size to  $32 \times 32$  and the learning rate to  $10^{-5}$  in all experiments. For the independent diffusion models on CIFAR-10 and CelebA datasets, we train them separately for 50 and 20 epochs, respectively, using a batch size of 128. To embed the watermark, which contains only one sample, we train the model from scratch with the watermark embedding loss presented in 12 for 100 epochs on CIFAR-10 and 40 epochs on CelebA, respectively. The batch size remains 128 for each iteration, where the task and watermark data are split equally as 64. This setting ensures an equivalent iteration number on the task dataset between the independent and watermarked models. To embed the watermark by fine-tuning the pre-trained

Embedding Settings	WDM-selected	WDM-random
Baseline(CIFAR-10)	$53.23 \pm 0.01$	$53.23 \pm 0.01$
TFS(CIFAR-10)	$52.70 \pm 0.11$	$53.52 \pm 0.42$
FT(CIFAR-10)	$57.10 \pm 0.22$	$55.97 \pm 0.45$
Baseline(CelebA)	$26.44 \pm 0.61$	$26.44 \pm 0.61$
TFS(CelebA)	$23.82 \pm 0.12$	$23.70 \pm 0.05$
FT(CelebA)	$26.14 \pm 0.34$	$24.47 \pm 0.20$

Table 4: The fidelity of watermarked DMs evaluated by the FID score in different configurations for MNIST as the watermark data. Results are represented in the mean value with corresponding variance format.

Embedding Settings	WDM-selected		WDM-random	
	WS $\downarrow$ (FID)	VC $\downarrow$ (p-value)	WS $\downarrow$ (FID)	VC $\downarrow$ (p-value)
Baseline(CIFAR-10)	343.84	$10^{-1}$	311.62	$10^{-1}$
TFS(CIFAR-10)	8.10	$10^{-11}$	12.79	$10^{-12}$
FT(CIFAR-10)	11.84	$10^{-11}$	18.22	$10^{-11}$
Baseline(CelebA)	314.74	$10^{-1}$	319.31	$10^{-1}$
TFS(CelebA)	15.27	$10^{-13}$	13.51	$10^{-12}$
FT(CelebA)	11.19	$10^{-12}$	15.03	$10^{-15}$

Table 5: Results for the detectability of the WDM in different configurations for MNIST as the watermark data.

independent model, we fine-tune it using the loss with an additional 50 epochs on CIFAR-10 and 20 epochs on CelebA, respectively, with a batch size of 128, where the task data and watermark data are split equally. The trigger factor is set to  $\gamma_1 = 0.8$ , and the trade-off factor for task training and watermark embedding is set to  $\gamma_2 = 1$ .

## D. MNIST as the Watermark Data

In this section, we consider embedding the watermark distribution as the MNIST which has a non-zero variance. In practice, we use the MNIST training dataset as the watermark dataset to embed, which contains multiple samples. We first present the fidelity of watermarked model with different embedding configurations in Table. 4. The degradation in fidelity caused by the WDM is not significant in both trigger settings, which keeps the same as the results in the setting that watermark data contains only one sample.

The watermark detectability results for the WDM with different configurations are presented in Table. 5. Compared to the experiments, the detectability of embedded watermark is represented using FID scores instead of the MSE scores. We can observe that the watermark similarity mean  $\mu_s$  of recovered target watermark data is significantly smaller than that from an independent model  $\mu_c$ , both in WDM-selected and WDM-random settings. The p-values of both configurations through training from scratch and fine-tuning are below the typical significance level of  $10^{-3}$  in the one-side hypothesis test. It indicates that the null hypothesis  $H_0$  can be rejected with a high enough significance, demonstrating the embedded watermark's detectability.

The results of the WDM against model compression attacks are presented in Table. 6. It can be observed that the watermark similarities from the compressed watermarked DMs have no significant degradation compared with those from the watermarked DMs. The p-values are still below the significance level, which indicates the robustness of the WDM against the model compression attack in our settings.

Embedding Settings	WDM-selected		WDM-random	
	$\Delta WS \downarrow$ (FID)	$VC \downarrow$ (p-value)	$\Delta WS \downarrow$ (FID)	$VC \downarrow$ (p-value)
TFS(CIFAR-10)	0.0267	$10^{-11}$	0.0802	$10^{-14}$
FT(CIFAR-10)	0.0364	$10^{-11}$	0.0874	$10^{-12}$
TFS(CelebA)	0.2323	$10^{-13}$	0.1441	$10^{-14}$
FT(CelebA)	0.0894	$10^{-12}$	0.0170	$10^{-12}$

Table 6: Results of watermark similarities and verification confidence for WDM against model compression attacks in different configurations.

The results of the WDM against model compression attacks are presented in Table. 6. It can be observed that the watermark similarities from the compressed watermarked DMs have no significant degradation compared with those from the watermarked DMs. The p-values are still below the significance level, which indicates the robustness of the WDM against the model compression attack in our settings.